NATURAL FRACTURE CHARACTERIZATION AT THE UTAH FORGE EGS TEST SITE: DISCRETE NATURAL FRACTURE NETWORK, STRESS FIELD, AND CRITICAL STRESS ANALYSIS

by Bryan Forbes[1], Joseph N. Moore[1], Aleta Finnila[2], Robert Podgorney[3], Siavash Nadimi[4], and John D. McLennan[4]

[1]Energy & Geoscience Institute, University of Utah, Salt Lake City, Utah
[2]Golder Associates, Redmond, Washington
[3]Idaho National Laboratory, Idaho Falls, Idaho
[4]Department of Chemical Engineering, University of Utah, Salt Lake City, Utah

Miscellaneous Publication 169-N
Utah Geological Survey
a division of
UTAH DEPARTMENT OF NATURAL RESOURCES

This paper is part of *Geothermal Characteristics of the Roosevelt Hot Springs System and Adjacent FORGE EGS Site, Milford, Utah*. https://doi.org/10.34191/MP-169

Bibliographic citation:

Forbes, B., Moore, J.N., Finnila, A., Podgorney, R., Nadimi, S., and McLennan, J.D., 2019, Natural fracture characterization at the Utah FORGE EGS test site—discrete natural fracture network, stress field, and critical stress analysis, *in* Allis, R., and Moore, J.N., editors, Geothermal characteristics of the Roosevelt Hot Springs system and adjacent FORGE EGS site, Milford, Utah: Utah Geological Survey Miscellaneous Publication 169-N, 11 p., https://doi.org/10.34191/MP-169-N.

NATURAL FRACTURE CHARACTERIZATION AT THE UTAH FORGE EGS TEST SITE: DISCRETE NATURAL FRACTURE NETWORK, STRESS FIELD, AND CRITICAL STRESS ANALYSIS

by Bryan Forbes, Joseph N. Moore, Aleta Finnila, Robert Podgorney, Siavash Nadimi, and John D. McLennan

ABSTRACT

Natural fractures are pre-existing cracks in a rock created from changes in earth stresses over time. In oil, gas, and geothermal operations, natural fractures can dominate fluid flow patterns, lead to unanticipated stress shadowing effects, drilling stability issues, and complex interactions with hydraulically induced fractures. These challenges can have perverse production and fluid flow effects on a reservoir. All formations contain unique sets of natural discontinuities. Therefore, it is highly desirable to locate and characterize natural fractures to assist in determining their associated contributions or risks to producing a quality reservoir.

Well 58-32 in Milford, Utah, was drilled to a depth of 7550 ft to serve as the pilot well for the Utah Frontier Observatory for Research in Geothermal Energy (FORGE) site. Formation Micro-Imager (FMI) logs and outcrop maps were used as the primary measurement sources for characterizing natural fracture properties such as their type, orientation, geometry, conductivity, and connectivity. This paper describes three activities incorporating natural fractures to characterize the FORGE test site reservoir: 1) construction of a discrete fracture network (DFN) to stochastically characterize natural fractures away from well control, 2) determination of the field stresses, and 3) analysis of natural fracture critical stresses at the well borehole. This work describes initial tasks completed during FORGE Phase 2B and will be extended to further refine and improve the understanding of the test site during Phase 2C.

INTRODUCTION

The Utah FORGE (Frontier Observatory for Research in Geothermal Energy) site was chosen by the Department of Energy (DOE) as the winning location for testing and demonstrating new technologies that will advance geothermal heat extraction from naturally fractured, low-permeability host rocks—in particular, enhanced geothermal systems (EGS) energy development (Simmons et al., 2016). The test site is located 250 km south of Salt Lake City and 16 km north-northeast of Milford, Utah (Figure 1), between the Basin and Range and Colorado Plateaus. During Phase 2B of the FORGE project, a pilot well, 58-32, was drilled, completed, and tested. Tests and measurements from the well were used to characterize the reservoir and support the FORGE site as the best EGS development candidate.

A successful thermal reservoir incorporates hydraulic stimulation techniques to propagate tensile fractures and/or to reactivate pre-existing shear fractures that often reorient to favor extensile propagation (Ye and Ghassemi, 2018). All reservoirs contain unique sets of natural fractures. These naturally occurring discontinuities are often composed of complex networks that affect the rock conductivity, mechanical properties, and preferred fluid flow pathways (Elmo and Stead, 2010; Nadimi et al., 2016). Natural fractures can cause unanticipated interactions between hydraulic fractures, drilling stability issues, complex fluid paths, and contact interactions with hydraulically induced fractures. Natural fracture characterization is common in the oil, gas, and mining industries and is becoming frequently incorporated in geothermal systems to help predict, avoid, and mitigate drilling, completion, and reservoir development issues (Xia et al., 2017).

The importance of natural fractures in subsurface characterization has influenced the development of various natural fracture modeling tools (Herbert, 1996). Today, models can incorporate 3D stochastically-generated natural fracture networks that honor the measured parameter ranges compiled from data sets which can be 1D (e.g., well FMI data), 2D (e.g., outcrop data) or 3D (e.g., seismic data). A combination of data measured from well 58-32 was used to develop probabilistic representations of in situ fractures, known as a discrete fracture network (DFN) (Dershowitz et al., 2004; Meyer and Bazan, 2011). The rationale for developing a DFN in Phase 2B is to consider the mechanical effects natural fractures have on the granitic reservoir.

In this study, a stochastic DFN model of the FORGE site was built using data measurements from well 58-32. Formation Micro-Imager (FMI) logs and outcrops maps were used as the primary inputs in characterizing natural fracture properties such as their

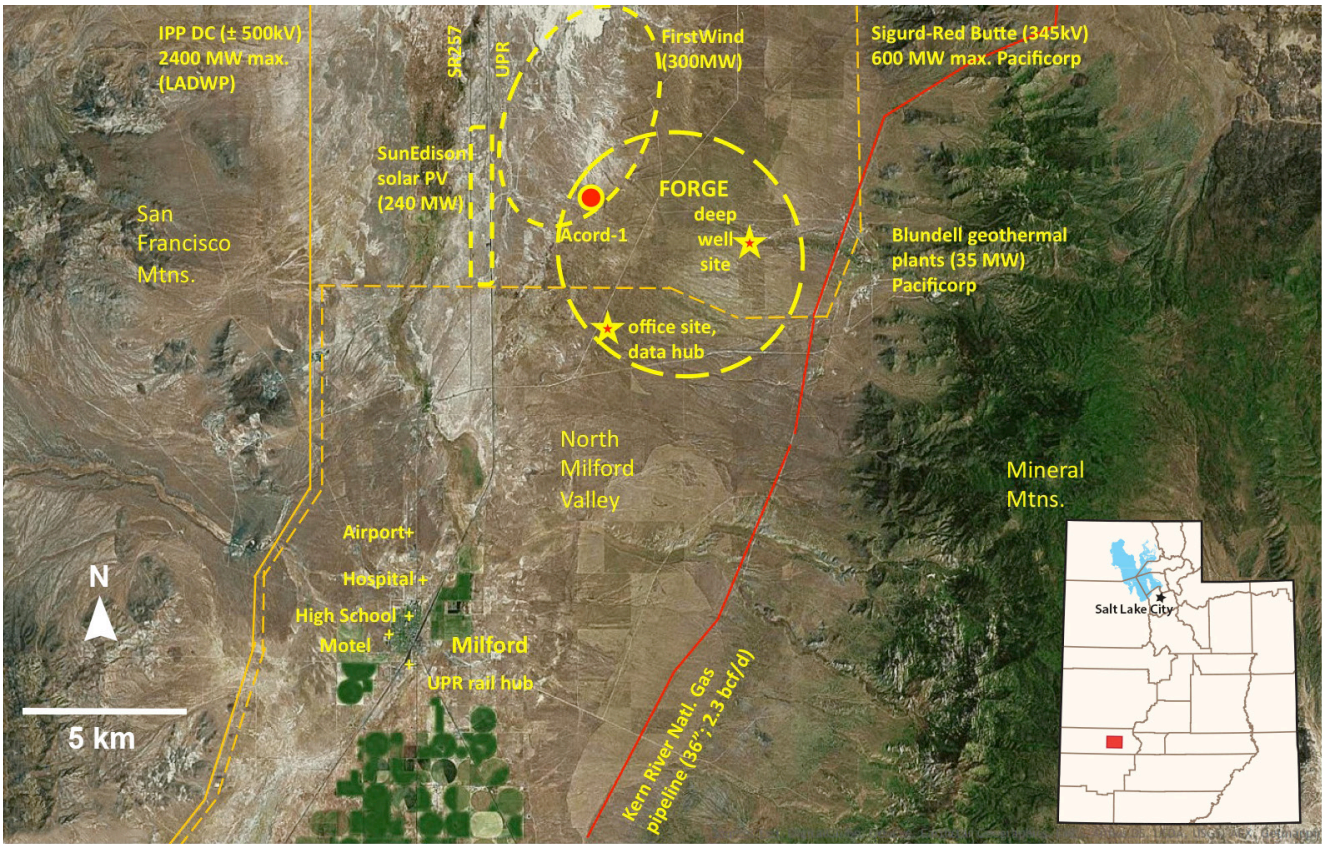

Figure 1. *Location of the FORGE deep well site near Milford, Utah (Allis et al. 2016).*

classification type, orientation, geometry, conductivity, and fracture connectivity. Additionally, various cycles of injection data were analyzed to determine the stress fields. The in situ stresses and wellbore fractures identified from the FMI logs were implemented in a stress analysis tool. The tool was used to identify fractures that were close to being critically stressed and likely to open first during hydraulic fracture stimulation. This information will be highly beneficial for designing optimal hydraulic fracture injection and reservoir management approaches for the wells planned to be drilled in Phase 2C of the FORGE project.

Discrete Fracture Network (DFN)

Well 58-32 was drilled, completed, and tested in 2017 to determine the crystalline granitic reservoir properties at the Utah Milford FORGE site. Outcrop mapping, seismic surveys, well logging, microhydraulic fracturing, pressure transient analysis, and core testing provided the intrinsic information for building a representative DFN. In particular, FMI data recorded in well 58-32 was processed. Each individual natural fracture was classified according to its orientation and fracture type. The FMI fractures were identified and categorized based on the resistivity differences observed along the rock as follows:

- Resistive continuous – partially open fractures filled with resistive materials such as calcite and quartz that limit fluid flow.
- Conductive continuous – an open conductive fracture around the borehole likely to be a preferred fluid flow path.
- Conductive partially resistive – partially open fractures with varying resistivity around the wellbore. Fracture fluid flow may be possible if calcite and quartz removal techniques are implemented (wellbore acid wash, for example).

Conductive partially resistive fractures constitute 97% of the natural fracture sample size. The fracture orientations from the image processing fall into three major groups with the following general strikes: N-S, E-W, and NE-SW groupings. Approximately 2000 natural features were identified over the entire logging interval of a baseline FMI run. Drilling-induced fractures were excluded from the imaged data, focusing the DFN construction on natural fractures. Natural fractures identifiable by the FMI are shown in rose and stereonet plots in Figure 2 from 3176 ft measured depth [MD] to 7550 ft total depth [TD].

Outcrop fracture mapping provided guidance in determining DFN properties such as the length, persistence, and terminations of the fractures around well 58-32 (Figure 3). From a nearby outcrop in the Mineral Mountains, natural fracture trace data

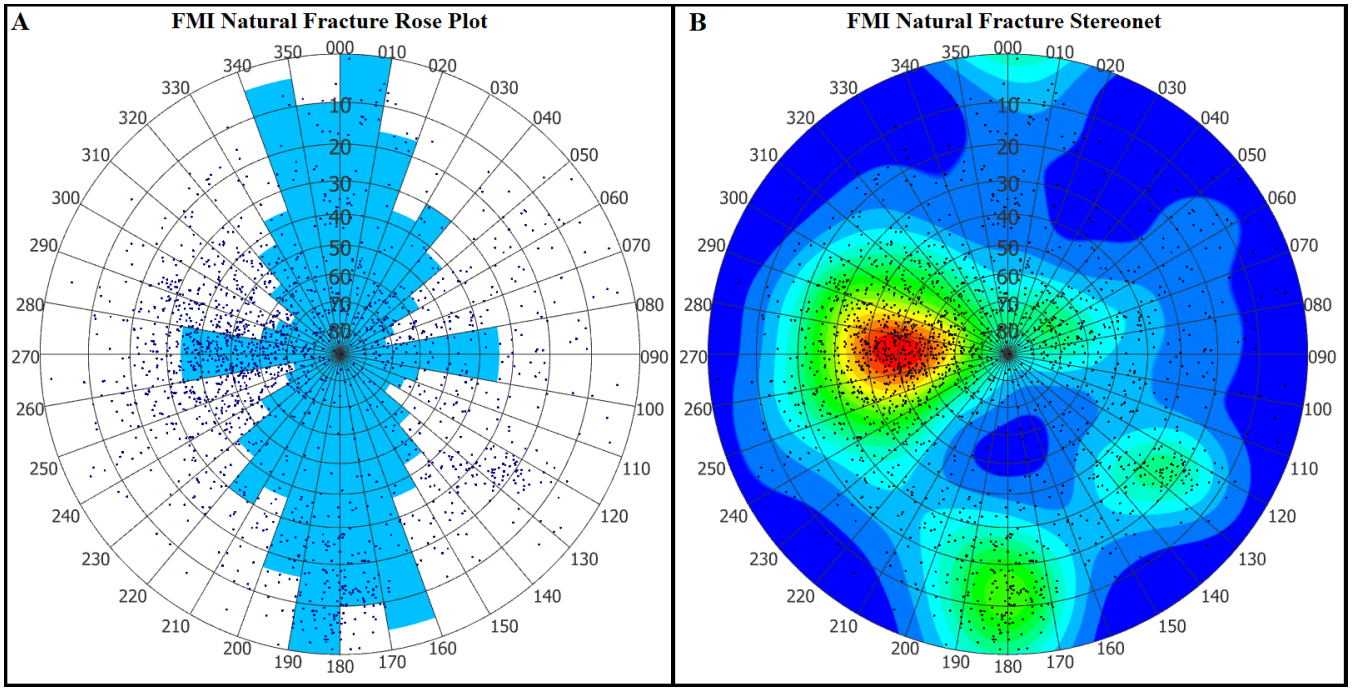

Figure 2. *Natural fractures identified from the FMI run from 3176 ft to 7550 ft TD in well 58-32.* ***(A)*** *The rose plot indicates the strike of the fractures.* ***(B)*** *The upper hemisphere, equal-angle stereonet plots the strike and dip of the natural fracture poles. Three general strike groups are identified: N-S, NE-SW, and a weak E-W group.*

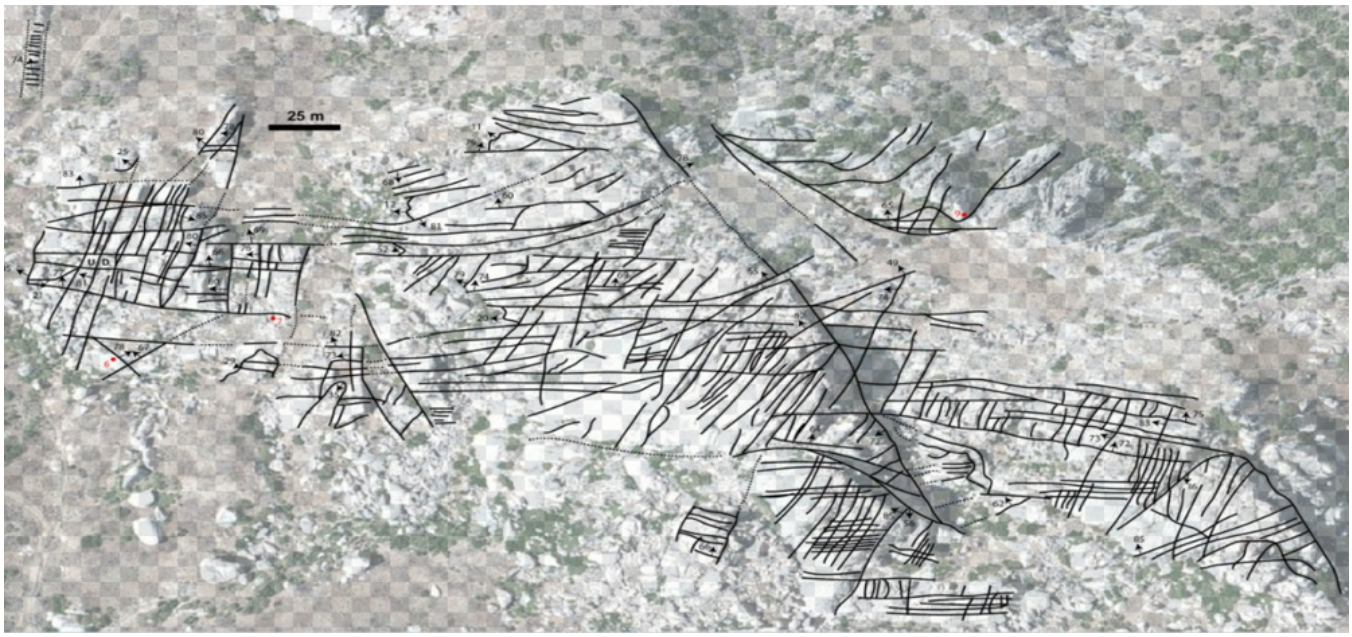

Figure 3. *Outcrop map from Salt Cove in the nearby Mineral Mountains where the target granite from the FORGE reservoir is exposed. The black lines represent mapped natural fractures superimposed on an aerial photograph. The strike, dip, and length of each fracture is recorded and used as one of the data sets for developing the FORGE site stochastic DFN. The surface location of well 58-32 is outside of this photograph (approximately 8 km west). Similar mapping was conducted for other outcrops, denoted as Bailey Springs, Negro Mag North, and Blundell SE.*

(strike, dip, and length) were fitted to the scale of the outcrop map, allowing determination of the equivalent fracture size corresponding to each exposed fracture trace. The fracture size is the radius of a circular fracture having the same area as the actual fracture shape. The measured fracture trace length will therefore be equal to or less than twice the fracture size (circular fracture diameter) depending on how the outcrop surface intersects the fracture. Figure 3 shows one of multiple outcrop maps used in determining DFN properties.

DFN models require inputs such as mean and standard deviation to generate statistically representable fracture properties. Fracture size can be estimated by constructing a cumulative frequency plot that shows the percentage of trace lengths that are less than or equal to particular values. A distribution curve is fit to the cumulative frequency plot that has the closest resemblance to the dataset (significance value). Figure 4 shows a cumulative frequency plot of the length data taken from the outcrop in Figure 3. A log-normal distribution gave the best match to the data (95% significance). The Salt Cove fracture size mean and standard deviation are 92 ft and 75 ft, respectively. This fitting procedure was also carried out for the other outcrop datasets. Note that while the trace length data best fit a log-normal distribution, this measured distribution can also represent data sets following an actual power law distribution that are truncated at both the low and high ends of the range.

Discrete fracture network models are not exact representations of all the actual fractures in the full 3D reservoir. A DFN can match the exact fracture locations and orientations measured in the wellbore or from outcrops. However, it is important to remember that DFNs also stochastically generate natural fractures away from measured areas using statistical inputs derived from direct field measurements.

Fischer distribution parameters were calculated for the N-S, E-W, and NE-SW fracture sets using the data provided from the FMI and outcrop evaluations. Table 1 shows the distribution data used to stochastically generate the fracture sets. The Fisher distribution in Table 1 is the analog of the Normal (Gaussian) distribution for a sphere, and is used to account for multiple uncorrelated variations in rock properties and stress conditions that can cause variations in the fracture orientation. The K1 value is a concentration parameter. An increasing K1value produces a higher distribution of fractures around the mean trend and plunge.

The vertical and areal dimensions of the DFN generation region were selected to cover the entirety of the FORGE site, resulting in an approximately 1 km^3 modeling domain. The stochastic natural fracture density and orientations were compared against the FMI fractures measured to determine the validity of the population datasets being generated. The statistical routine in FracMan™ generated approximately 350,000 fractures in the modeling domain. Each generated fracture set was filtered to only include approximately 2000 fractures directly intersecting the well. These filtered, intersecting fractures were compared with the fractures detected by the FMI survey before any injection tests were performed in the wellbore. The stochastic DFN models honored the FMI datasets and showed enough statistic similarity to represent the 1 km^3 region.

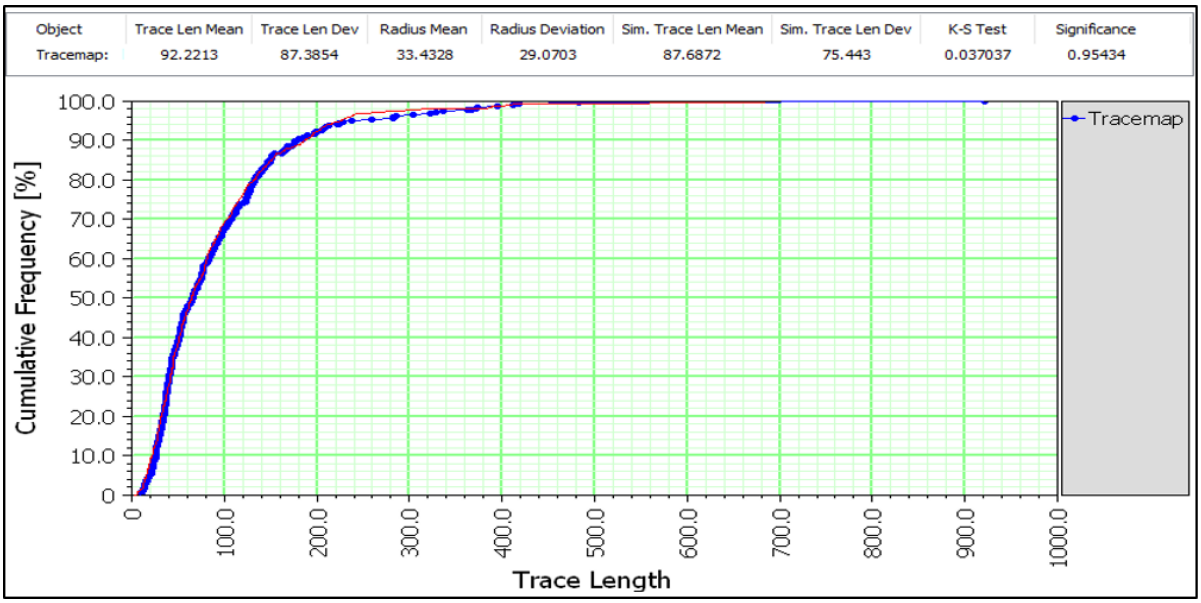

Figure 4. *Central Mineral Mountain cumulative frequency plot (trace lengths are displayed in meters). For example, 50% of the trace lengths measured are less than approximately 60 m. The blue points are the measured fracture lengths of natural fractures mapped in the Salt Cove outcrop in Figure 2. A line (red) is fit to the dataset and extracts mean and standard deviation values used to statistically represent the outcrop fracture lengths during DFN construction.*

Table 1. *Fracture set generation parameters and their distribution.*

	Orientation (fracture pole)			Fracture Radius (ft)		Fracture Intensity
Fracture Set	Fisher Distribution			Log Normal Distribution		(# Fractures / ft)
	Mean Trend (°)	Mean Plunge (°)	K1 Value	Mean	Standard Deviation	
NE/SW	331	1.0	.98	92	82	3.1
N/S	87	41.8	41.8	105	94	1.2
E/W	3	10.8	10.8	115	98	0.32

Field Stress Measurements

Stress and permeability measurements were made in late September 2017 in 147 ft of open hole below the 7-inch casing shoe. The 7-inch, 29-lb-per-ft, N80 casing was set at a total measured depth of 7374.9 ft kelly bushing (KB). After waiting on cement and a cement bond log (CBL), the hole was cleaned to 7525 ft (originally, drilled to 7536 ft). The purpose of leaving 10 ft of cement at the base of the well was to allow logging to total depth after injection. After the injection program, the cement was drilled out to allow full run of the FMI and dipole sonic imaging (DSI) logging tools.

Before injection, Baker Hughes ran a Retrievamatic™ compression packer into the hole. The setting depth covered 7244.7 to 7247.7 ft MD KB. A stinger was placed below the packer and communicated with the 4-inch drill pipe used to run the packer. At the bottom of the stinger was a gauge carrier for a pressure and temperature gauge, set to recover data every three seconds. Ports connecting to the openhole section were at 7426.8 ft MD (perforated sub). The stinger deployed a DiDrill™ pressure and temperature tool in the openhole section, allowing for a reliable bottomhole pressure and temperature measurement at 7426.8 ft MD, 7418.7 ft true vertical depth (TVD) KB. Tubing pressure, annulus pressure and injection rate were recorded by the pumping services company, Resource Cementing, and an auxiliary pressure transducer was provided by the mud loggers, West Coast Geologic. The drill pipe was tested successfully to 8000 psi. A rupture disk downhole was removed by progressively dropping a sinker bar. This disk allowed pressure testing of the drill pipe without pressurizing the formation.

Figures 5 and 6 show a surface pressure chronology for the injection measurements made over a two-day period. Table 2 shows the sequence of injection measurements made on September 22 and 23, 2017. The injection protocols were as follows.

September 22, 2017:

1) Injection/falloff test to assess permeability.
2) Three cycles of microfracturing for stress determination.
3) Diagnostic fracture injection test (DFIT) at ~5.8 and 8.7 barrels per minute (bpm) with an extended shut-in to determine permeability.

September 23, 2017:

1) One cycle repeating the microhydraulic fracturing for stress determination.
2) Step rate and DFIT with an extended shut-in to determine permeability.
3) DFIT followed by a proppant stage with 200-mesh calcium carbonate to prop the fracture and enhance differentiation between fractures identified with the pre- and post-fracturing FMI logging.

Table 3 summarizes the calculated stress gradients. The maximum stress gradient was determined using methods proposed by Haimson and Fairhurst (1967). Tensile strength is set to zero assuming pre-existing fracturing. Near-wellbore pore pressure was taken as hydrostatic (as determined from the near-static wellbore pressure, measured before injection began). Instead of using breakdown pressure, fracture reopening pressure was taken as the initial deviation from linearity during the injection phase of each cycle. All measurements were expressed as gradients based on the true vertical depth of the bottom hole pressure device (7429 ft KB MD, 7421 ft KB TVD) The depth can be corrected to ground level by subtracting 21.5 feet from the TVD value, but

is inconsequential. The vertical stress was inferred by integrating the logging-based density values to the surface. The suggested stress field ranges are the following:

σ_{hmin}.....0.58–0.63 psi/ft (best guess 0.62 psi/ft)

σ_{HMAX}.....0.68–0.82 psi/ft (best guess 0.77 psi/ft)

σ_{v}.....1.13 psi/ft

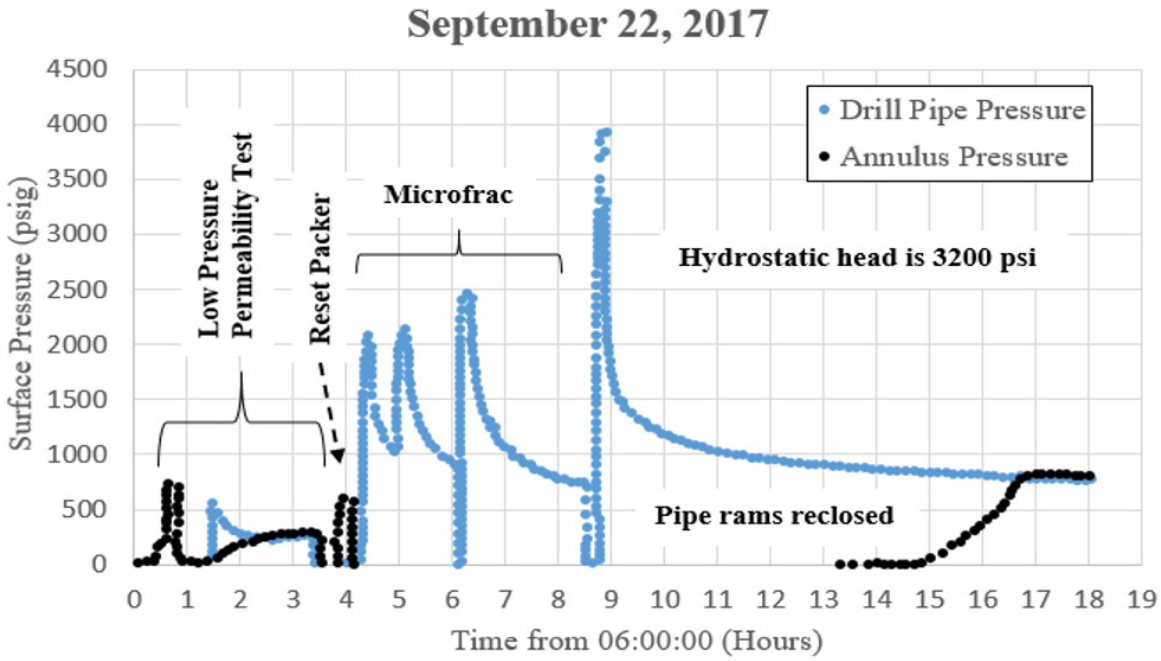

Figure 5. *Surface pressure during the injection campaign. The plot shows the injection program on September 22, 2017. Five injection cycles are shown (cycles 1 through 5, chronologically increasing).*

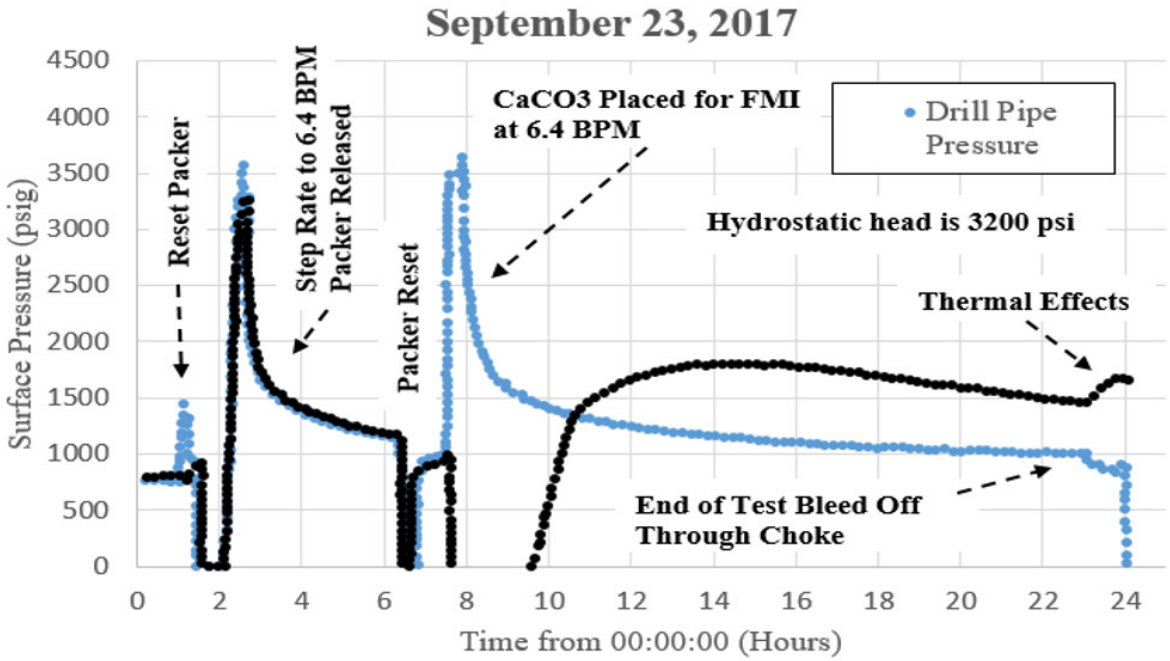

Figure 6. *Surface pressure during the injection campaign. The plot shows the injection program on September 23, 2017. Three injection cycles are shown (cycles 6 through 8, chronologically increasing).*

Table 2. *Summary of stress and permeability measurements.*

Cycle	Description	Purpose
1	Injection falloff. Pressure was increased to below the pressure required to hydraulically fracture the formation.	Assessment of native permeability before hydraulic fracturing testing
2	Microhydraulic fracture. 2.8 bbl were pumped at 0.4 bpm	Stress measurement
3	Microhydraulic fracture. 4.2 bbl were pumped at 0.4 bpm	Stress measurement
4	Microhydraulic fracture. 10.0 bbl were pumped at 0.8 bpm	Stress and permeability measurements
5	DFIT™ pumped initially at 5.8 bpm and increased to 8.7 bpm for 5 minutes (67.2 barrels pumped). Prolonged shut-in.	Stress and permeability measurements
6	Repeat microhydraulic fracture test. 0.4 bpm and 3.8 bbl pumped	Stress measurement
7	76.9 bbl were pumped in a Step Rate Test (SRT) where rate was progressively increased • 0.4 bpm, 2.7 bbl pumped • 0.8 bpm, 4.1 bbl pumped • 1.6 bpm, 9.8 bbl pumped • 3.2 bpm, 16.1 bbl pumped • 6.3 bpm, 44.2 bbl pumped	An SRT is alternative method for evaluating minimum in situ stress as a function of injection rate. Shut-in pressure decline at the end of the SRT can be used to pick fracture closure with classic techniques. Permeability was also inferred.
8	DFIT™ containing an 8 bbl slug of viscosified fluid carrying 200-mesh calcium carbonate proppant. 28.8 bbl of water at 6.4 bpm, followed by 8 bbl of viscosified xanthan with $CaCO_3$ at 6.4 bpm, displaced with 3 bbl of water at 6.4 bpm, and 8 bbl of water at 3 bpm to encourage screenout and fracture packing for subsequent logging.	Stress and permeability measurements

Table 3. *Summary of reopening data.*

Cycle	Description	Maximum Rate (bpm)	Volume Pumped (bbl)	Inflection (psi)	Inflection Gradient (psi/ft)	σ_{HMIN} Gradient (psi/ft)	σ_{HMAX} Gradient (psi/ft)	Temperature at Shut-In (°F)
1	Injection falloff							319
2	Micro-hydraulic fracture	0.4	3.8	4751	0.64	0.620	0.79	326
3	Micro-hydraulic fracture	0.4	4.2	4900	0.66	0.711	0.80	326
4	Micro-hydraulic fracture	0.8	10	5308	0.71	0.656	0.82	321
5	DFIT	8.7	67.2	4681	0.63	0.731	0.79	270
6	Micro-hydraulic fracture	0.4	3.8	4163	0.56	0.605	0.78	333
7	SRT	6.3	76.9	5205	0.70	0.75	0.82	280
8	DFIT with slug	6.7	86.6	5989	0.81	0.633	0.78	240

Critical Stress Analysis and Hydro-Shearing

The orientation of critically stressed fractures during hydro-shearing stimulation was studied using the Critical Stress Analysis functionality in FracMan™. The proposed approach is similar to Finnila et al. (2015). The analysis assumes shear failure occurs if the shear force,$|\tau|$ exceeds the shear strength, $f(\sigma)$, of a fracture if (Dershowitz et al., 1998):

$$|\tau| \geq f(\sigma) \tag{1}$$

If the fracture is critically stressed, its permeability may be enhanced. The Mohr-Coulomb criterion is used to calculate the fracture shear strength of fractures:

$$f(\sigma) = S_0 + \sigma \tan \phi_f \tag{2}$$

S_0 is the cohesion of the fracture, σ is the shear stress, and ϕ_f is the friction angle. Critically stressed fractures are typically oriented at a $(45° + {}^{\phi_f}/_2)$ angle from the minimum principal stress direction, σ_3 (Goodman, 1989).

The deepest 1000 ft of well 58-32 was analyzed from 6550 to 7550 ft to determine which fractures were critically stressed. The vertical, maximum, and minimum horizontal stress gradients considered were 1.13, 0.77, and 0.62 psi/ft, respectively (the basis for these stress gradients is explained in Section 3). Figure 7 shows the natural fracture stresses over the 1000 ft interval. Red colored fractures are less stable and should slip first. The first column in Figure 7 is the critical stress value calculated for each fracture at hydrostatic pore pressure (approximately 3200 psi). No fractures are critically stressed under static conditions. The next three columns show stable fractures in blue and critically stressed fractures in red for pressures of 200, 400 and 600 psi above hydrostatic pressure.

Predictions of which fractures will fail first can be tested by isolating and stimulating sections of the well. Stable sections (blue colors in the first column of Figure 7) remain closed and do not increase fracture conductivity after low-pressure stimulation (below the minimum principal stress). Conversely, sections containing fractures near to being critically stressed (red colors in the first column) are predicted to show an increase in fracture conductivity during low-pressure stimulation. The Mohr diagrams for the four different pore pressure cases are shown in Figure 8. A rose plot of critically stressed fractures at 600 psi excess pore pressure is shown in Figure 9. The critically stressed fracture directions from the rose plot suggest NE-SW-azimuth fractures are likely to be critically stressed first and could be considered as initial targets during hydraulic fracture stimulation.

CONCLUSIONS

Recent industry research has focused on incorporating natural fractures into reservoir characterization. The presence of natural fractures can cause challenges during drilling, completions, and production in an enhanced geothermal system. Outcrop and well 58-32 FMI data show that the FORGE granitic reservoir houses multiple, complex natural fracture sets.

A stochastic discrete fracture network model was constructed that honors the FORGE Phase 2B data and covers the entire test site boundaries. Injection tests were conducted and used to determine the local stresses in well 58-32. Stress values were used in critical stress analysis to predict natural fractures likely to fail first during hydraulic fracture stimulation. Results showed that NE-SW-azimuth fractures have the highest likelihood of re-opening first. This information will be important for future hydraulic fracture injection design and reservoir management tasks in Phase 2C.

In summary, this study provides: 1) initial stochastic natural fracture models of the FORGE site, 2) an approach for determining the granitic reservoir local stress field using well injection data, and 3) an analysis of critically stressed fractures near the 58-32 wellbore. As mentioned, caution must be taken when developing a DFN model. The fractures are not exact representations of all the actual fractures in the full 3D reservoir and are dependent on the data available. As Phase 2C progresses, the work described in this paper during Phase 2B will be refined to further characterize and develop the Utah FORGE EGS research site.

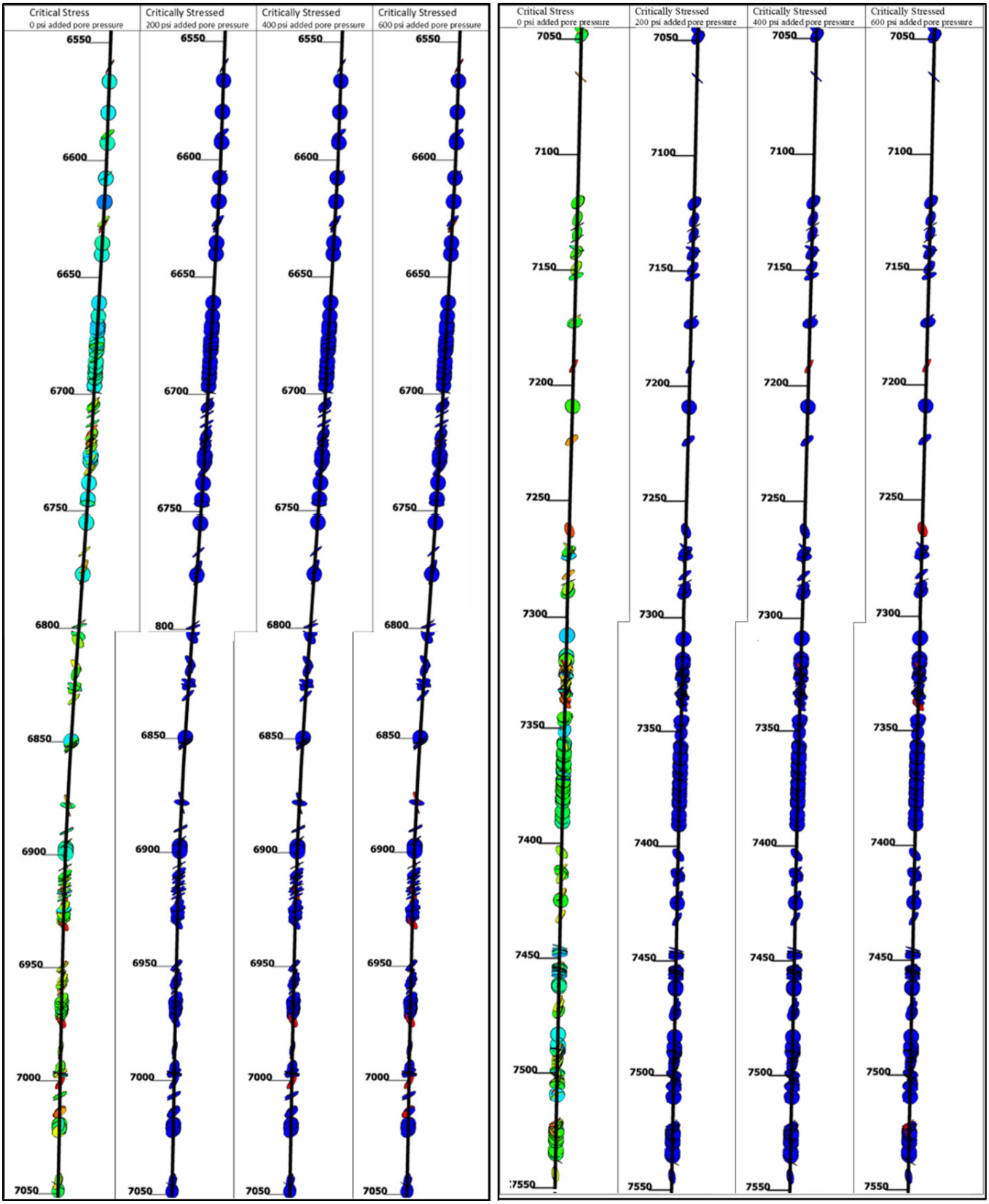

Figure 7. *The critical stress value calculated for each fracture identified from the FMI between 6550 ft to 7550 ft in the Utah 58-32 well. A hydrostatic and three overpressure instances were tested: 0 psi (hydrostatic ~3200 psi), 200 psi, 400 psi, and 600 psi. Red and orange highlighted fractures are under the highest degree of stress and most likely to open first during stimulation compared to the lower stressed blue fractures.*

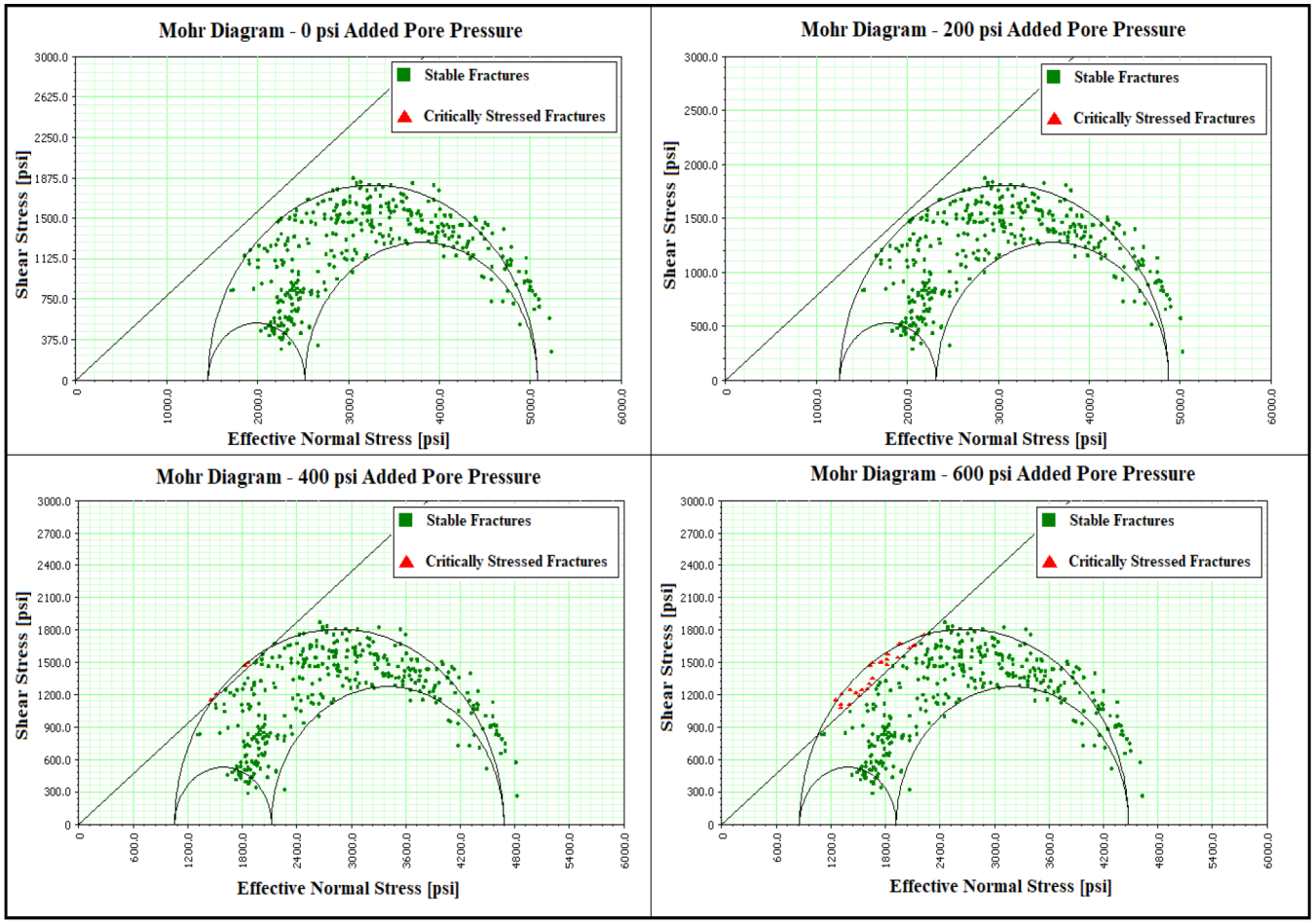

Figure 8. *Mohr diagram of the hydro-sheared system at varying pore pressure tests. Critically stressed fractures (red) are shown at a stimulation level between hydrostatic pore pressure and pore pressures approaching the minimum principal stress.*

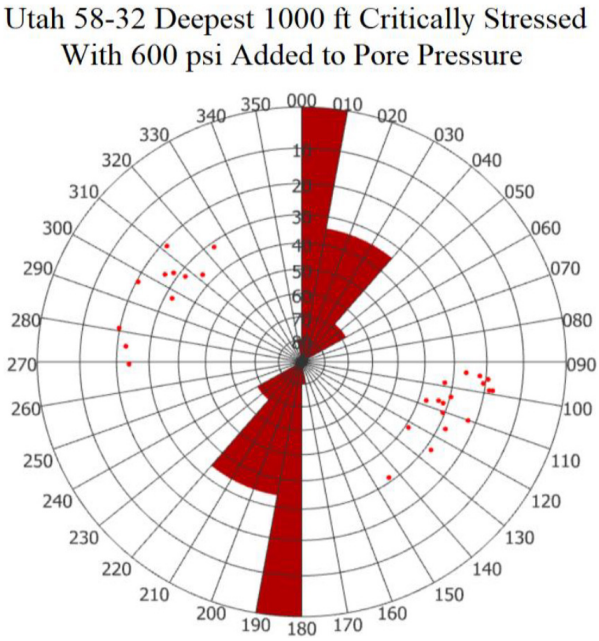

Figure 9. *Rose plot of critically stressed fractures at 600 extra psi pore pressure (fracture poles shown in upper hemisphere, equal angle stereonet). The majority of critically stressed fractures are oriented in the NE-SW direction that is approximate to the maximum horizontal stress direction.*

ACKNOWLEDGMENTS

Funding for this work was provided by the U.S. DOE under grant DE-EE0007080 "Enhanced Geothermal System Concept Testing and Development at the Milford City, Utah, FORGE Site". We thank the many stakeholders who are supporting this project, including Smithfield (Murphy Brown LLC), Utah School and Institutional Trust Lands Administration, and Beaver County as well as the Utah Governor's Office of Energy Development.

REFERENCES

Allis, R., Moore, J., Davatzes, N., Gwynn, M., Hardwick, C., Kirby, S., McLennan, J., Pankow, K., Potter, S., and Simmons, S., 2016, EGS concept testing and development at the Milford, Utah FORGE site. In Proceedings.

Dershowitz, B., LaPointe, P., Eiben, T., and Wei, L., 1998, Integration of Discrete Feature Network Methods with Conventional Simulator Approaches. Society of Petroleum Engineers, https://doi.org/10.2118/49069-MS.

Dershowitz, W.S., La Pointe, P.R., and Doe, T.W., 2004, Advanced in Discrete Fracture Network Modeling.

Elmo, D., and Stead, D., 2010, An integrated numerical modelling–discrete fracture network approach applied to the characterization of rock mass strength of naturally fractured pillars. Rock Mechanics and Rock Engineering, 43(1), p. 3–19.

Finnila, A., Dershowitz, W.S., Doe, T.W., and McLaren, R., 2015, Hydro-Shearing and Hydraulic Fracturing for Enhanced Geothermal Systems in Archetypical Normal, Strike-Slip, and Thrust Faulting Terrains, GRC, Geothermal Resources Council Annual Meeting. Vol 39, p. 303–314.

Goodman, R.E., 1989, Introduction to Rock Mechanics, Second Edition. John Wiley & Sons.

Haimson, B., and Fairhurst, C., 1967, Initiation and Extension of Hydraulic Fractures in Rocks, Society of Petroleum Engineers. https://doi.org/10.2118/1710-PA.

Herbert, A.W., 1996, Modelling approaches for discrete fracture network flow analysis, Developments in Geothechnical Engineering. Elsevier, Vol 79, p. 213–229.

Meyer, B.R., and Bazan, L.W., 2011, A discrete fracture network model for hydraulically induced fractures-theory, parametric and case studies, In SPE hydraulic fracturing technology conference, Society of Petroleum Engineers.

Nadimi, S., Miscovic, I., and McLennan, J., 2016, A 3D peridynamic simulation of hydraulic fracture process in a heterogeneous medium, Journal of Petroleum Science and Engineering, 145, p. 444–452.

Simmons, S., Kirby, S., Jones, C., Moore, J., Allis, R., Brandt, A., and Nash, G., 2016, The Geology, Geochemistry, and Geohydrology of the FORGE Deep Well Site, Milford, Utah, PROCEEDINGS, 41st Workshop on Geothermal Reservoir Engineering.

Xia, Y., Plummer, M., Mattson, E., Podgorney, R., and Ghassemi, A., 2017, Design, modeling, and evaluation of a doublet heat extraction model in enhanced geothermal systems, Renewable energy, 105, p. 232–247.

Ye, Z., and Ghassemi, A., 2018, Experimental study on injection-induced fracture propagation and coalescence for EGS stimulation, In Proc., 43rd Workshop on Geothermal Reservoir Engineering. Stanford, CA: Stanford Univ.